


Quantum-catalysis-enhanced extractable energy in a qubit quantum battery

Shun-Cai Zhao ¹, *

¹*Center for Quantum Materials and Computational Condensed Matter Physics,
Faculty of Science, Kunming University of Science and Technology, Kunming, 650500, PR China*

(Dated: Wednesday 29th April, 2026)

In realistic open-system environments, decoherence and dissipation naturally drive quantum batteries toward passive states, thereby limiting their maximum extractable work (ergotropy). While quantum catalysis has been proposed to mitigate this degradation, the underlying thermodynamic mechanism remains not fully understood. Here, we investigate a driven qubit quantum battery coherently coupled to a harmonic-oscillator catalyst, subject to simultaneous dephasing and dissipation. By employing the differential first law of open quantum thermodynamics, we analyzed the dynamic energy balance to separate work and heat contributions during the charging process. We find that the catalyst induces a transient negative energy flux (energy backflow) into the qubit. This backflow actively counteracts decoherence-induced passivation and drives the battery into highly non-passive states, resulting in a pronounced enhancement of the ergotropy. Furthermore, we quantitatively establish the physical connection between this transient negative energy flux and the ergotropy gain. These results identify this transient negative energy flux as the operative thermodynamic mechanism, providing concrete physical insights for optimizing quantum energy-storage devices in noisy environments.

PACs: 42.50.Gy

Keywords: quantum catalysis; qubit quantum battery; harmonic oscillator catalyst; extractable energy; external-field-driven

I. INTRODUCTION

The rapid development of quantum thermodynamics [1–5] has established quantum batteries (QBs) [6–11] as a centerpiece for high-efficiency nanoscale energy storage [12–16]. The performance of a QB is primarily characterized by its *ergotropy*—the maximum extractable work via cyclic unitary operations [17–20]—and its instantaneous charging power. In parallel, quantum catalysis (QC) [21–26], where an auxiliary system facilitates state transformations without suffering a net change in its own resources [27–30], has emerged as a robust tool for enhancing QB performance.

A pivotal challenge for practical QBs is their inevitable coupling to dissipative environments, which induces dephasing and energy relaxation [31–34]. Such open-system dynamics drive the battery toward *passive states*, effectively suppressing the extractable work [3, 10]. While previous studies have utilized catalytic-like mechanisms to mitigate this degradation through spectral restructuring and supermode formation [22, 27, 35–41], these global dynamical interpretations often obscure the underlying *local* thermodynamic processes. Specifically, a

microscopic understanding of how a catalyst counteracts the entropy production and passivation at the subsystem level—particularly under non-energy-dissipative noise—remains largely elusive. Without resolving the transient energy fluxes, a rigorous link between catalytic dynamics and ergotropy gain cannot be established, hindering the formulation of predictive design principles for noisy environments.

In this work, we resolve this deficiency by revealing the microscopic thermodynamic mechanism driving catalysis-enhanced ergotropy. By analyzing the charging of a driven qubit QB coherently coupled to a harmonic-oscillator catalyst, we operate in the experimentally relevant *energy-invariant* regime, where the catalyst’s mean energy is conserved only at the end of the protocol [21, 22]. Using the differential formulation of the open-system first law ($dE = dW + dQ$), we perform a dynamic decomposition of local energy fluxes under simultaneous dephasing and dissipation.

Our central finding is that the catalyst facilitates a transient *negative local energy flux* ($J(t) < 0$) into the battery subsystem, acting as a coherent energy backflow. This backflow structurally counteracts dephasing-induced passivation, maintaining the qubit in a highly non-passive state and yielding a substantial ergotropy en-

* Corresponding author: zhaosc@kust.edu.cn.

hancement. We quantitatively establish the causal link between this integrated negative flux and the net ergotropy gain, identifying this backflow as the operative thermodynamic operative behind catalytic QBs.

The remainder of this paper is organized as follows. Sec. II introduces the physical model and formalizes the local thermodynamic quantities. Sec. III presents the results on transient flux mechanisms and ergotropy enhancement. Sec. IV provides a detailed thermodynamic analysis, followed by a proposed implementation in circuit quantum electrodynamics (cQED) in Sec. V. Finally, we conclude in Sec. VI.

II. PHYSICAL MODEL

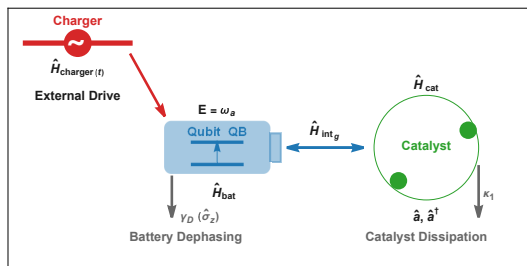


FIG. 1. Schematic of the externally driven qubit quantum battery (QB) operating in the charging phase. The QB is coherently coupled to an auxiliary harmonic-oscillator catalyst to enhance energy storage, while simultaneously being subjected to environmental dephasing and dissipation.

We study the charging stage of an open quantum battery composed of a target qubit and an auxiliary bosonic catalyst. The qubit is the subsystem in which useful energy is stored, while the catalyst is introduced as an additional quantum degree of freedom that can assist the charging dynamics and modify the amount of locally extractable work. Throughout this work, the term “catalyst” is used in an operational sense, namely, to denote an auxiliary subsystem that enhances the charging performance of the battery. Accordingly, the other components, including the quantum battery, external environment and driving field system, are collectively defined as the “battery system”. It does not, by itself, imply exact state recovery at all intermediate times.

Thus, the total Hamiltonian can be decomposed into two parts: \hat{H}_0 and \hat{H}_{Cat} ,

$$\begin{aligned} \hat{H}(t) &= \hat{H}_0 + \hat{H}_{\text{Cat}} \\ &= \hat{H}_{\text{QB}} + \hat{H}_{\text{int}} + \hat{H}_{\text{drive}}(t) + \hat{H}_{\text{Cat}}, \end{aligned} \quad (1)$$

where $\hbar = 1$. The bare Hamiltonian of the qubit battery is

$$\hat{H}_{\text{QB}} = \frac{\omega_a}{2} \hat{\sigma}_z, \quad (2)$$

with transition frequency ω_a . The catalyst is modeled as a single harmonic oscillator(HO),

$$\hat{H}_{\text{Cat}} = \omega_c \hat{a}^\dagger \hat{a}, \quad (3)$$

where ω_c is the oscillator frequency and \hat{a} (\hat{a}^\dagger) is the annihilation (creation) operator. The qubit and the catalyst are coupled through a Jaynes-Cummings interaction,

$$\hat{H}_{\text{int}} = g(\hat{\sigma}^+ \hat{a} + \hat{\sigma}^- \hat{a}^\dagger), \quad (4)$$

with coupling strength g . This form assumes the rotating-wave approximation and is appropriate in the weak-coupling, near-resonant regime. Charging is induced by a classical drive applied directly to the qubit,

$$\hat{H}_{\text{drive}}(t) = \Omega \sin(\omega_d t) \hat{\sigma}_x, \quad (5)$$

where Ω and ω_d denote the drive amplitude and driving frequency, respectively.

The initial state is chosen as

$$\hat{\rho}(0) = |0\rangle_{\text{QB}} \langle 0| \otimes |0\rangle_{\text{Cat}} \langle 0|, \quad (6)$$

so that the battery starts from its ground state and has zero initial ergotropy. The subsequent dynamics are described by the Lindblad master equation

$$\frac{d\hat{\rho}}{dt} = -i[\hat{H}(t), \hat{\rho}] + \mathcal{L}[\hat{\rho}], \quad (7)$$

with

$$\mathcal{L}[\hat{\rho}] = \sum_k \gamma_k \left(\hat{L}_k \hat{\rho} \hat{L}_k^\dagger - \frac{1}{2} \{ \hat{L}_k^\dagger \hat{L}_k, \hat{\rho} \} \right). \quad (8)$$

We include two dissipative channels: pure dephasing of the qubit and damping of the catalyst mode. Unless stated otherwise, the corresponding jump operators are taken as

$$\hat{L}_\phi = \frac{\hat{\sigma}_z}{\sqrt{2}}, \quad \hat{L}_\kappa = \hat{a}, \quad (9)$$

with rates γ_D and κ_1 , respectively. With the convention in Eq. (9), γ_D directly gives the decay rate of the off-diagonal coherence of the qubit density matrix. While local Lindblad master equations are known to exhibit thermodynamic inconsistencies in the steady-state limit under strong coupling, our investigation is strictly confined to the ultrafast transient charging regime. On this short timescale, the local approach remains robust and accurately captures the initial coherent energy exchange prior to the onset of global environmental dressing.

The reduced state of the battery is

$$\hat{\rho}_{\text{QB}}(t) = \text{Tr}_{\text{Cat}}[\hat{\rho}(t)]. \quad (10)$$

To quantify the useful energy stored in the battery, we evaluate the ergotropy of the reduced qubit state,

$$\mathcal{E}(t) = \text{Tr}[\hat{\rho}_{\text{QB}}(t)\hat{H}_{\text{QB}}] - \text{Tr}[\hat{\rho}_{\text{passive}}(t)\hat{H}_{\text{QB}}], \quad (11)$$

where $\hat{\rho}_{\text{passive}}(t)$ is the passive state associated with $\hat{\rho}_{\text{QB}}(t)$ [5, 7, 42]. Since our interest is the performance of the qubit itself as a local work-storage unit, we focus on the ergotropy of the reduced battery state rather than on global work extraction from the full composite system.

To monitor the role of the catalyst, we also evaluate its instantaneous energy,

$$E_{\text{Cat}}(t) = \text{Tr}[\hat{\rho}_{\text{Cat}}(t)\hat{H}_{\text{Cat}}], \quad (12)$$

where

$$\hat{\rho}_{\text{Cat}}(t) = \text{Tr}_{\text{QB}}[\hat{\rho}(t)]. \quad (13)$$

In addition, the local energy current into the battery is defined as

$$\mathcal{J}(t) = \text{Tr}\left[\frac{d\hat{\rho}_{\text{QB}}(t)}{dt}\hat{H}_0\right]. \quad (14)$$

As detailed in Appendix A, since \hat{H}_{QB} is time independent, Eq. (14) can be written as

$$\mathcal{J}(t) = -i \text{Tr}\left(\hat{\rho}(t)[\hat{H}_{\text{QB}}, \hat{H}_{\text{int}} + \hat{H}_{\text{drive}}(t)]\right) + \text{Tr}\left[\hat{H}_{\text{QB}}\mathcal{L}[\hat{\rho}(t)]\right]. \quad (15)$$

This expression separates the drive-induced, interaction-mediated, and dissipative contributions to the local energy variation of the battery, and it will be used below to analyze the mechanism by which the catalyst modifies the charging process.

All frequencies and dissipation rates are expressed in units of ω_a . The master equation is solved numerically using an adaptive-step ordinary-differential-equation integrator. For the bosonic catalyst, a finite Fock-space

	ω_a	ω_c	Ω	ω_d	g	κ_1	γ_D
Fig.2,3(a)	2.0	/	0.5	2.0	0.75	0.5	0.05
Fig.2,3(b)	2.0	0.01	0.5	2.0	/	0.2	0.05
Fig.2,3(c)	2.0	0.01	0.5	2.0	0.75	/	0.05
Fig.2,3(d)	2.0	0.01	0.5	2.0	0.75	0.2	/

TABLE I. Simulation parameters used in Figs. (2) and (3). Note that all frequency parameters are presented in consistent arbitrary units (e.g., scaled relative to a reference energy scale setting $\hbar = 1$).

truncation N_c is introduced, and all reported results are verified to be converged with respect to further increases of N_c . Unless otherwise stated in the figure captions, the parameter values used in the simulations are listed in Table I.

In the following, we are primarily interested in how the catalyst modifies the local charging dynamics and the ergotropy of the qubit battery under coherent driving and dissipation.

III. RESULTS

A. Uncatalyzed ergotropy dynamics

We first analyze the reference charging protocol in the absence of the HO catalyst. In this case, the dynamics reduce to those of a driven qubit battery subject only to pure dephasing. The corresponding open-system evolution is generated by the dephasing dissipator, which, following the structure implied by Eq. (8) and standard Lindblad form, takes the form:

$$\mathcal{L}_{\text{deph}}[\hat{\rho}] = \gamma_D (\hat{\sigma}_z \hat{\rho} \hat{\sigma}_z - \hat{\rho}), \quad (16)$$

with jump operator $\hat{L}_D = \hat{\sigma}_z$. Here γ_D denotes the qubit dephasing rate.

The uncatalyzed ergotropy is shown by the red dashed curves in all panels of Fig. 2. Starting from the initially discharged state specified in Sec. II, the external resonant drive first builds up extractable energy in the qubit, leading to transient oscillations in $\mathcal{E}(t)$. At later times, pure dephasing suppresses the coherence required to sustain non-passive population inversion, and the ergotropy correspondingly decreases toward a lower long-time value. Thus, even though pure dephasing does not directly remove energy from the qubit, it degrades the drive-assisted generation of non-passive states and substantially reduces the accessible extractable work.

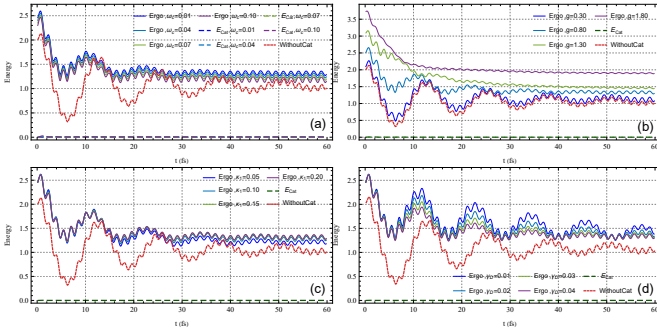


FIG. 2. (Color online) Time evolution of the qubit ergotropy $\mathcal{E}(t)$ with and without the catalyst during the charging stage. Panel (a) varies the catalyst frequency ω_c , panel (b) the qubit-catalyst coupling strength g , panel (c) the catalyst damping rate κ_1 , and panel (d) the qubit dephasing rate γ_D . The red dashed curve in each panel denotes the uncatalyzed protocol, while the colored solid curves correspond to the catalyzed protocol. The thin dashed curve in each panel closes to zero indicate the catalyst energy $E_{\text{Cat}}(t)$, which remains nearly unchanged on the scale of the figure.

B. Catalysis-enhanced ergotropy

We now turn to the catalyzed charging protocol. The dynamics of the coupled qubit-catalyst system are governed by the full master equation with

$$\mathcal{L}[\hat{\rho}] = \mathcal{L}_{\text{cat}}[\hat{\rho}] + \mathcal{L}_{\text{deph}}[\hat{\rho}], \quad (17)$$

where

$$\mathcal{L}_{\text{cat}}[\hat{\rho}] = \kappa_1 \left(\hat{a}\hat{\rho}\hat{a}^\dagger - \frac{1}{2} \{ \hat{a}^\dagger\hat{a}, \hat{\rho} \} \right), \quad (18)$$

and $\mathcal{L}_{\text{deph}}[\hat{\rho}]$ is given by Eq. (16).

A useful diagnostic of the catalytic regime is the oscillator energy

$$E_{\text{Cat}}(t) = \text{Tr} \left[\hat{\rho}(t) \hat{H}_{\text{Cat}} \right]. \quad (19)$$

As indicated by the thin dashed curves in Fig. 2, $E_{\text{Cat}}(t)$ remains close to zero and varies only weakly throughout the evolution for the parameter range explored here. This behavior is consistent with an *energy-invariant* catalytic regime [21, 22], in which the auxiliary mode facilitates the charging process while storing only a negligible amount of energy on average. We stress, however, that approximate constancy of the catalyst energy does not by itself imply exact recovery of the catalyst state; the present evidence therefore supports an energetic notion of approximate catalysis rather than a strict state-invariant one.

The colored solid curves in Fig. 2 show that introducing the catalyst can noticeably enhance the qubit ergotropy over the uncatalyzed reference. In panels (a) and (b), the enhancement depends sensitively on both the catalyst frequency ω_c and the qubit-catalyst coupling strength g , indicating that the catalytic benefit is strongest in a restricted resonance and coupling window. Within this regime, the catalyst increases not only the peak ergotropy but also the time interval over which the battery remains appreciably non-passive.

We further examine the robustness of this enhancement against environmental noise. Figs. 2(c) and 2(d) display the ergotropy dynamics for different values of the catalyst damping rate κ_1 and the qubit dephasing rate γ_D , respectively. Over the parameter range considered here, the catalyzed protocol consistently yields a larger ergotropy than the uncatalyzed one. This trend suggests that the auxiliary oscillator does more than simply provide an additional transient energy-exchange channel: it modifies the open-system charging dynamics in a way that helps preserve the qubit's non-passive character. To clarify this point, we next analyze the associated energy-flow decomposition.

IV. THERMODYNAMIC ANALYSIS OF CATALYTIC ENHANCEMENT

To gain further insight into the origin of the enhanced ergotropy, we now analyze the local energy balance of the qubit battery within the differential formulation of the first law of open quantum thermodynamics. Our goal is not to claim a complete microscopic reconstruction of the mechanism from thermodynamic observables alone, but rather to identify a consistent thermodynamic signature correlated with the catalyst-assisted maintenance of non-passive battery states.

A. Quantum first law and local energy-flow convention

We define the internal energy of the battery with respect to the Hamiltonian \hat{H}_0 , in direct correspondence with the ergotropy definition in Eq. (11):

$$E_{\text{QB}}(t) = \text{Tr} \left[\hat{\rho}_{\text{QB}}(t) \hat{H}_0 \right], \quad (20)$$

where $\hat{\rho}_{\text{QB}}(t) = \text{Tr}_{\text{Cat}}[\hat{\rho}(t)]$ is the reduced density operator of the qubit. The differential first law for the reduced

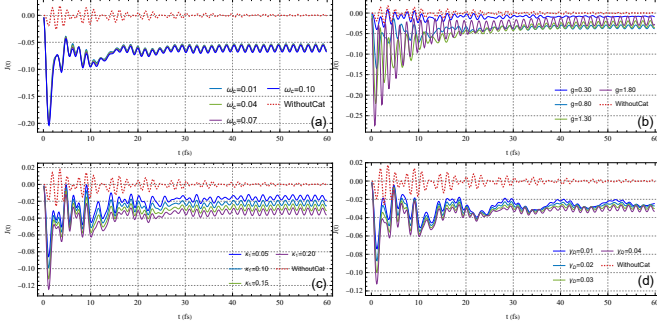


FIG. 3. (Color online) Time evolution of the heat current $J(t)$ for the qubit battery. The red dashed curve denotes the uncatalyzed protocol, and the colored solid curves denote the catalyzed protocol. Panel (a) varies the catalyst frequency ω_c , panel (b) the coupling strength g , panel (c) the catalyst damping rate κ_1 , and panel (d) the qubit dephasing rate γ_D . Unless explicitly varied, the remaining parameters are fixed to the values listed in Table I. Time is measured in fs, and $J(t)$ is reported in the corresponding energy-per-time units implied by the Hamiltonian parameters. Negative values of $J(t)$ indicate inward heat flow into the reduced qubit subsystem under the convention adopted in Eq. (23).

subsystem is then written as[43–46]

$$\frac{d}{dt}E_{\text{QB}}(t) = \dot{W}(t) + \dot{Q}(t) = P(t) + J(t), \quad (21)$$

where $P(t)$ denotes the power injected by the explicitly time-dependent drive, and $J(t)$ denotes the generalized energy current, which encompasses both the irreversible heat dissipation to the environment and the coherent energy exchange with the catalyst. In the present decomposition,

$$P(t) = \dot{W}(t) = \text{Tr} \left[\hat{\rho}_{\text{QB}}(t) \frac{d\hat{H}_0}{dt} \right], \quad (22)$$

and

$$J(t) \equiv \dot{Q}(t) = \text{Tr} \left[\frac{d\hat{\rho}_{\text{QB}}(t)}{dt} \hat{H}_0 \right]. \quad (23)$$

With this sign convention, $J(t) < 0$ corresponds to an effective inward energy flux into the reduced battery subsystem.

We emphasize that this local decomposition(Eq.(15)) is adopted as a diagnostic tool for the driven open-system dynamics. In particular, within a Markovian Lindblad framework, a transient negative $J(t)$ should be interpreted as a local thermodynamic signature of inward energy flow into the qubit subsystem under the chosen partition, rather than as direct evidence of non-Markovian

reservoir memory. This distinction is important because the catalyst-induced effect discussed below originates from coherent battery-catalyst coupling superimposed on Markovian dissipation.

B. Dynamics of the energy flux

Fig. 3 shows the time evolution of $J(t)$ for the uncatalyzed and catalyzed protocols. The numerical results were obtained using the stiff solver described in Sec. II. We verified that the reported dynamics are stable against the chosen timestep parameters and the low-excitation truncation of the oscillator Hilbert space in the parameter regime relevant to Fig. 3; additional numerical details may be provided in the *Code availability* VI if needed.

For the uncatalyzed protocol (red dashed curves), the qubit is subject only to external driving and pure dephasing. In this case, $J(t)$ remains close to zero, with only small oscillatory corrections. This behavior is consistent with the fact that pure dephasing does not itself constitute an energy-relaxation channel for the bare qubit Hamiltonian. Instead, its role is to suppress the coherence generated by the drive, thereby indirectly limiting the build-up of non-passive states and reducing the attainable ergotropy, as seen in Fig. 2.

By contrast, the catalyzed protocol exhibits a qualitatively different short-time response. In all four panels of Fig. 3, the colored solid curves display an initial interval during which $J(t) < 0$, indicating an effective inward heat current into the reduced qubit subsystem. The magnitude and duration of this negative-current window depend on the catalyst frequency ω_c , the coupling strength g , the catalyst damping rate κ_1 , and the qubit dephasing rate γ_D . Within the explored parameter range, stronger catalytic enhancement of ergotropy is consistently associated with a more pronounced negative-current transient.

This transient negative heat current provides a useful thermodynamic signature of the catalyst-assisted charging process. Physically, the coherent qubit-catalyst interaction enables the auxiliary mode to reshape the local energy-exchange pathways experienced by the qubit during the driven evolution. As a result, the qubit can temporarily receive energy in a way that helps counteract the dephasing-induced suppression of non-passivity. At later times, the oscillation amplitude decreases and $J(t)$ approaches a small value near zero, indicating that the dominant catalytic contribution is a transient rather than indefinitely growing effect.

Comparing Figs. 2 and 3, we find a clear dynamical correlation between the early-time negative-current window and the subsequent enhancement of $\mathcal{E}(t)$. In parameter regimes where the negative excursion of $J(t)$ is more pronounced, the qubit typically reaches and maintains a higher ergotropy. We therefore interpret the transient negative heat current as a thermodynamic indicator closely associated with the catalyst-induced preservation of non-passive battery states. While this does not by itself exhaust the full microscopic mechanism, it does provide a consistent and quantitatively accessible explanation for why the catalyzed protocol outperforms the uncatalyzed one in the present open-system setting.

Overall, the energy-flow analysis supports the conclusion that the auxiliary oscillator can enhance qubit-battery performance by inducing a transient inward heat current into the reduced battery subsystem, thereby helping the driven qubit remain farther from passivity in the presence of dephasing.

V. PROPOSED EXPERIMENTAL REALIZATION VIA CIRCUIT QUANTUM ELECTRODYNAMICS

The theoretical framework and thermodynamic mechanisms unveiled in this work strongly motivate an immediate experimental implementation using state-of-the-art circuit quantum electrodynamics (cQED) architectures [47–49]. Here, we outline a feasible experimental protocol to quantitatively verify the transient energy backflow and its causal role in catalytic quantum battery (QB) enhancement.

The proposed setup comprises a superconducting transmon qubit functioning as the QB, which is strongly coupled to a high-quality superconducting microwave resonator acting as the quantum catalyst (HO). To ensure near-zero thermal occupancy of the environmental bath, the device must operate in a dilution refrigerator at millikelvin temperatures ($T \sim 10$ mK). In a typical resonant charging scenario, the fundamental frequencies are tuned to $\omega_{\text{QB}}/2\pi \approx \omega_{\text{HO}}/2\pi \sim 5.0$ GHz. The essential energy backflow mechanism is facilitated by the Jaynes-Cummings (JC) interaction. Operating in the strong-coupling regime requires the JC coupling rate to be $g/2\pi \sim 50$ -100 MHz, which significantly dominates over the intrinsic qubit dephasing rate ($\gamma_D/2\pi \sim 0.1$ MHz). The cavity decay rate κ_1 can be engineered via a tunable coupler or a Purcell filter, allowing it to vary over an order of magnitude (e.g., 0.5 to 5 MHz) to test the

robustness of the catalytic advantage against dissipation.

The operational protocol proceeds in three main stages: initialization, coherent charging, and projective measurement. Initially, both the QB and the HO are actively reset to their respective ground states, preparing the joint state $|g\rangle_{\text{QB}} \otimes |0\rangle_{\text{HO}}$ with high fidelity. During the charging phase, a resonant microwave drive is applied to the QB via a local drive line for a variable duration t_{ch} . Following the charging pulse, the instantaneous reduced density matrix of the battery, $\hat{\rho}_{\text{QB}}(t_{\text{ch}})$, is reconstructed using time-resolved quantum state tomography (QST). This is achieved by measuring the Pauli observables $\langle \hat{\sigma}_x \rangle$, $\langle \hat{\sigma}_y \rangle$, and $\langle \hat{\sigma}_z \rangle$ through standard dispersive readout techniques, averaged over a large ensemble of experimental repetitions. The ergotropy $\mathcal{E}(t_{\text{ch}})$ is then directly evaluated from the reconstructed $\hat{\rho}_{\text{QB}}(t_{\text{ch}})$.

The most critical challenge lies in resolving the transient thermodynamic fluxes, specifically the heat current $J(t)$. According to the first law of open quantum thermodynamics, this flux is inferred via $J(t) = dE_{\text{QB}}(t)/dt - P(t)$. The internal energy is obtained from the inversion population as $E_{\text{QB}}(t) = \frac{\hbar\omega_{\text{QB}}}{2} \langle \hat{\sigma}_z(t) \rangle$, while the input charging power is precisely defined by the microwave drive Hamiltonian as $P(t) = \text{Tr}[\hat{\rho}_{\text{QB}}(t) \dot{\hat{H}}_{\text{drive}}(t)]$. Since numerical differentiation of QST data is highly susceptible to measurement shot noise, the discrete time-series data of $E_{\text{QB}}(t)$ must be fitted to a physically informed smooth envelope prior to taking the derivative dE_{QB}/dt .

A definitive experimental demonstration of the quantum catalytic mechanism proposed herein necessitates three concurrent observations. First, the inferred heat current must exhibit a transient, unambiguously negative profile ($J(t) < 0$) during the early charging dynamics (on the timescale of $t \sim 1/g \approx$ tens of nanoseconds), indicating energy backflow from the HO. Second, this negative flux must temporally coincide with a substantially higher measured ergotropy $\mathcal{E}(t)$ compared to an identical control experiment performed without the HO catalyst. Finally, to strictly satisfy the thermodynamic definition of a catalyst, partial state tomography of the HO must confirm state recovery at the end of the charging cycle; that is, the final state of the cavity must exhibit a near-unity fidelity with its initial vacuum state, $\mathcal{F}(\hat{\rho}_{\text{HO}}(t_{\text{final}}), |0\rangle\langle 0|_{\text{HO}}) \approx 1$.

Successful execution of this protocol would not only validate the fundamental predictions of transient thermodynamic backflow but also establish a concrete technological blueprint for deploying noise-resilient quantum energy-storage devices.

VI. CONCLUSIONS

In conclusion, we have elucidated the microscopic thermodynamic mechanism driving catalysis-enhanced charging in a driven qubit quantum battery (QB) under open-system dynamics. By partitioning the local energy flux according to the quantum first law, we demonstrate that the catalyst functions as a coherent thermodynamic buffer. It induces a transient negative heat flux ($J(t) < 0$) that acts as a coherent energy backflow into the battery subsystem, effectively counteracting decoherence-induced passivation and driving the QB into highly non-passive configurations with enhanced ergotropy.

This framework establishes that the catalyst can synthesize beneficial non-Markovian-like backflow dynamics even in strictly dissipative environments, providing a robust blueprint for noise-resilient quantum energy storage. Future research may extend this mechanism to many-body architectures and non-Gaussian catalytic resources to explore the scaling limits of collective quantum charging and absolute thermodynamic bounds. These investigations, coupled with the proposed circuit QED implementations, will facilitate the practical deployment of high-performance quantum thermodynamic technologies.

Acknowledgments.— This work is supported by the National Natural Science Foundation of China (Grant Nos. 62065009 and 61565008), Yunnan Fundamental Research Projects, China(Grant No. 2016FB009).

CODE AVAILABILITY

This manuscript has associated data in a data repository. [Author' comment: All data included in this manuscript are available upon reasonable request by contacting with the corresponding author]. The Supporting Information is available free of charge at: [Codes-for-Quantum-catalysis-enhanced-extract-energy](#)

Appendix A: Derivation of the local energy current

We start from the definition of the local energy current flowing into the qubit battery (QB),

$$\mathcal{J}(t) = \text{Tr} \left[\frac{d\hat{\rho}_{\text{QB}}(t)}{dt} \hat{H}_0 \right], \quad (\text{A1})$$

where $\hat{\rho}_{\text{QB}}(t) = \text{Tr}_{\text{Cat}}[\hat{\rho}(t)]$ is the reduced density matrix of the qubit subsystem. The total Hamiltonian of the system is given by

$$\begin{aligned} \hat{H}(t) &= \hat{H}_0 + \hat{H}_{\text{Cat}} \\ &= \hat{H}_{\text{QB}} + \hat{H}_{\text{int}} + \hat{H}_{\text{drive}}(t) + \hat{H}_{\text{Cat}}, \end{aligned} \quad (\text{A2})$$

where we define a subsystem Hamiltonian

$$\hat{H}_0 = \hat{H}_{\text{QB}} + \hat{H}_{\text{int}} + \hat{H}_{\text{drive}}(t). \quad (\text{A3})$$

Substituting Eq.(A3) into Eq.(A1)

$$\mathcal{J}(t) = \text{Tr} \left[\dot{\hat{\rho}}_{\text{QB}} \left(\hat{H}_{\text{QB}} + \hat{H}_{\text{int}} + \hat{H}_{\text{drive}} \right) \right]. \quad (\text{A4})$$

The time evolution of the total density matrix is governed by the Lindblad master equation,

$$\frac{d\hat{\rho}(t)}{dt} = -i[\hat{H}(t), \hat{\rho}(t)] + \mathcal{L}[\hat{\rho}(t)], \quad (\text{A5})$$

where $\hat{H}(t)$ is the total Hamiltonian and $\mathcal{L}[\cdot]$ denotes the dissipator. By taking the partial trace over the degrees of freedom other than the QB, we obtain the equation of motion for the reduced density matrix:

$$\dot{\hat{\rho}}_{\text{QB}} = \text{Tr}_{\text{rest}} \left\{ -i[\hat{H}_{\text{QB}} + \hat{H}_{\text{int}} + \hat{H}_{\text{drive}} + \hat{H}_{\text{Cat}}, \hat{\rho}] + \mathcal{L}[\hat{\rho}] \right\}. \quad (\text{A6})$$

We assume that \hat{H}_{Cat} acts only on the environment/auxiliary space and commutes with the QB operations, leading to $\text{Tr}_{\text{rest}}[\hat{H}_{\text{Cat}}, \hat{\rho}] = 0$. Thus,

$$\dot{\hat{\rho}}_{\text{QB}} = -i\text{Tr}_{\text{rest}} \left[\hat{H}_{\text{QB}} + \hat{H}_{\text{int}} + \hat{H}_{\text{drive}}, \hat{\rho} \right] + \text{Tr}_{\text{rest}} \mathcal{L}[\hat{\rho}]. \quad (\text{A7})$$

Substituting $\dot{\hat{\rho}}_{\text{QB}}$ (A7) into $\mathcal{J}(t)$ (A4) and utilizing the cyclic property of the trace along with the partial trace property $\text{Tr}_{\text{QB}}[\text{Tr}_{\text{rest}}(\dots)\hat{H}_{\text{QB}}] = \text{Tr}[(\dots)\hat{H}_{\text{QB}}]$, we evaluate the commutator term. Specifically, focusing on the core coherent exchange term, we arrive at the final decomposed form:

$$\mathcal{J}(t) = -i \text{Tr} \left(\hat{\rho}(t) [\hat{H}_{\text{QB}}, \hat{H}_{\text{int}} + \hat{H}_{\text{drive}}(t)] \right) + \text{Tr} \left[\hat{H}_{\text{QB}} \mathcal{L}[\hat{\rho}(t)] \right]. \quad (\text{A8})$$

which corresponds to Eq. (15) and follows from the fact that $[\hat{H}_{\text{QB}}, \hat{H}_{\text{QB}}] = 0$ in the main text.

Remark.— This desired decomposition effectively separates the local energy current into two physical processes. The first term describes the coherent energy exchange induced by the interaction and the external drive, while the second term accounts for the dissipative energy flow due to the environment. It is worth noting that this decomposition is strictly dependent on the chosen subsystem partition and should be interpreted accordingly within the framework of open quantum thermodynamics.

-
- [1] H. Spohn, *Journal of Mathematical Physics* **19**, 1227 (1978).
- [2] D. Ferraro, M. Campisi, G. M. Andolina, V. Pellegrini, and M. Polini, *Phys. Rev. Lett.* **120**, 117702 (2018).
- [3] D. Farina, G. M. Andolina, A. Mari, M. Polini, and V. Giovannetti, *Phys. Rev. B* **99**, 035421 (2019).
- [4] F. Barra, *Phys. Rev. Lett.* **122**, 210601 (2019).
- [5] R. Alicki and M. Fannes, *Phys. Rev. E* **87**, 042123 (2013).
- [6] W.-L. Song, H.-B. Liu, B. Zhou, W.-L. Yang, and J.-H. An, *Phys. Rev. Lett.* **132**, 090401 (2024).
- [7] S. Seah, M. Perarnau-Llobet, G. Haack, N. Brunner, and S. Nimmrichter, *Phys. Rev. Lett.* **127**, 100601 (2021).
- [8] D. Rossini, G. M. Andolina, D. Rosa, M. Carrega, and M. Polini, *Phys. Rev. Lett.* **125**, 236402 (2020).
- [9] G. M. Andolina, D. Farina, A. Mari, V. Pellegrini, V. Giovannetti, and M. Polini, *Phys. Rev. B* **98**, 205423 (2018).
- [10] G. M. Andolina, M. Keck, A. Mari, M. Campisi, V. Giovannetti, and M. Polini, *Phys. Rev. Lett.* **122**, 047702 (2019).
- [11] W.-L. Song, J.-L. Wang, B. Zhou, W.-L. Yang, and J.-H. An, *Phys. Rev. Lett.* **135**, 020405 (2025).
- [12] X. Yang, Y.-H. Yang, M. Alimuddin, R. Salvia, S.-M. Fei, L.-M. Zhao, S. Nimmrichter, and M.-X. Luo, *Phys. Rev. Lett.* **131**, 030402 (2023).
- [13] K. V. Hovhannisyan, M. Perarnau-Llobet, M. Huber, and A. Acin, *Phys. Rev. Lett.* **111**, 240401 (2013).
- [14] F. C. Binder, S. Vinjanampathy, K. Modi, and J. Goold, *New J. Phys.* **17**, 075015 (2015).
- [15] F. Campaioli, F. A. Pollock, F. C. Binder, L. Celeri, J. Goold, S. Vinjanampathy, and K. Modi, *Phys. Rev. Lett.* **118**, 150601 (2017).
- [16] T. P. Le, J. Levinsen, K. Modi, M. M. Parish, and F. A. Pollock, *Phys. Rev. A* **97**, 022106 (2018).
- [17] H.-L. Shi, S. Ding, Q.-K. Wan, X.-H. Wang, and W.-L. Yang, *Phys. Rev. Lett.* **129**, 130602 (2022).
- [18] J.-Y. Gyhm, D. Safranek, and D. Rosa, *Phys. Rev. Lett.* **128**, 140501 (2022).
- [19] S. C. Zhao, Z. R. Zhao, and N. Y. Zhuang, *Phys. Rev. E* **112**, 024129 (2025).
- [20] W. Wu and J.-H. An, *Phys. Rev. Lett.* **133**, 050401 (2024).
- [21] P. Lipka-Bartosik, H. Wilming, and N. H. Y. Ng, *Rev. Mod. Phys.* **96**, 025005 (2024).
- [22] R. R. Rodriguez, B. Ahmadi, P. Mazurek, S. Barzanjeh, R. Alicki, and P. Horodecki, *Phys. Rev. A* **107**, 042419 (2023).
- [23] A. d. O. Junior, M. Perarnau-Llobet, N. Brunner, and P. Lipka-Bartosik, *Phys. Rev. Res.* **6**, 023127 (2024).
- [24] J. Aberg, *Phys. Rev. Lett.* **113**, 150402 (2014).
- [25] J. Eisert and M. Wilkens, *Phys. Rev. Lett.* **85**, 437 (2000).
- [26] D. Jonathan and M. B. Plenio, *Phys. Rev. Lett.* **83**, 3566 (1999).
- [27] G. A. Durkin, *Phys. Rev. A* **99**, 032315 (2019).
- [28] S. H. Lie and N. H. Y. Ng, *Phys. Rev. A* **108**, 012417 (2023).
- [29] P. Boes, J. Eisert, R. Gallego, M. P. Müller, and H. Wilming, *Phys. Rev. Lett.* **122**, 210402 (2019).
- [30] H. Yamasaki, S. Morelli, M. Miethlinger, J. Bavaresco, N. Friis, and M. Huber, *Quantum* **6**, 695 (2022).
- [31] A. Boudjemâa, L. Xu, and Q.-S. Tan, *Phys. Rev. A* **111**, 022443 (2025).
- [32] S. Roy and J. Gong, *Phys. Rev. B* **112**, 155409 (2025).
- [33] A. Passian, J. Dawson, S. Prowell, and W. Grice, *Phys. Rev. A* **111**, 042626 (2025).
- [34] P.-C. Kuo, S.-L. Yang, N. Lambert, J.-D. Lin, Y.-T. Huang, F. Nori, and Y.-N. Chen, *Phys. Rev. Res.* **7**, L012068 (2025).
- [35] B. Ahmadi, P. Mazurek, P. Horodecki, and S. Barzanjeh, *Phys. Rev. Lett.* **132**, 210402 (2024).
- [36] D. Rinaldi, R. Filip, D. Gerace, and G. Guarnieri, *Phys. Rev. A* **112**, 012205 (2025).
- [37] D. T. Hoang, F. Metz, A. Thomasen, T. D. Anh-Tai, T. Busch, and T. Fogarty, *Phys. Rev. Res.* **6**, 013038 (2024).
- [38] D. Qu, X. Zhan, H. Lin, and P. Xue, *Phys. Rev. B* **108**, L180301 (2023).
- [39] I. Henao and R. Uzdin, *Phys. Rev. Lett.* **130**, 020403 (2023).
- [40] T. Biswas, M. Lobejko, P. Mazurek, and M. Horodecki, *Phys. Rev. E* **110**, 044120 (2024).
- [41] C. A. Downing and M. S. Ukhtary, *Phys. Rev. A* **109**, 052206 (2024).
- [42] A. E. Allahverdyan, R. Balian, and T. M. Nieuwenhuizen, *Europhysics Letters* **67**, 565 (2004).
- [43] R. Alicki, *Journal of Physics A General Physics* **12**, L103 (1979).
- [44] W. Pusz and S. L. Woronowicz, *Communications in Mathematical Physics* **58**, 273 (1978).
- [45] P. Strasberg and A. Winter, *PRX Quantum* **2**, 030202 (2021).
- [46] B. d. L. Bernardo, *Phys. Rev. E* **102**, 062152 (2020).
- [47] D. Kafri, P. Adhikari, and J. M. Taylor, *Phys. Rev. A* **93**, 013412 (2016).
- [48] Y.-x. Liu, L. F. Wei, J. R. Johansson, J. S. Tsai, and F. Nori, *Phys. Rev. B* **76**, 144518 (2007).
- [49] S. Kotler, R. W. Simmonds, D. Leibfried, and D. J. Wineland, *Phys. Rev. A* **95**, 022327 (2017).